

# Comparing actual transpiration fluxes as measured at leaf-scale and calculated by a physically based agro-hydrological model

Ameneh Sobhani,<sup>1</sup> Shawkat B.M. Hassan,<sup>1</sup> Giovanna Dragonetti,<sup>2</sup> Raffaella Balestrini,<sup>3</sup> Mauro Centritto,<sup>3</sup> Antonio Coppola,<sup>1,4</sup> Alessandro Comegna<sup>1</sup>

<sup>1</sup>School of Agricultural, Forestry, Food and Environmental Sciences, University of Basilicata, Potenza; <sup>2</sup>Mediterranean Agronomic Institute of Bari, Land and Water Resources Management Division, Valenzano (BA); <sup>3</sup>Institute for Sustainable Plant Protection, National Research Council, Turin; <sup>4</sup>Department of Chemical and Geological Sciences, University of Cagliari, Monserrato (CA), Italy

## Abstract

The primary purpose of this paper is to compare the actual transpiration rates from tomato crops, as measured at leaf scale and estimated by a macroscopic approach in an agro-hydrological model named FLOWS, under variable soil properties and water availability. To this aim, sixteen plots were cultivated with tomatoes in Metaponto, Southern Italy. Soil hydraulic properties (SHP) were obtained using a fast *in situ* characterisation method. Leaf-area index (LAI) was measured using a leaf-area metre. SHP and LAI were then used in the physically-based FLOWS, which allowed calculating the macroscopic transpiration rates,  $T_{a,m}$ . Single-leaf transpiration rates,  $T_{a,l}$ , and stomatal conductance,  $g_{s,l}$ , were measured *in situ*. For comparison with  $T_{a,m}$ ,  $g_{s,l}$  was upscaled

by the Big-Leaf approach to canopy scale stomatal conductance,  $g_{s,c}$ , which was applied to the Penman-Monteith model to obtain the canopy-scale transpiration,  $T_{a,c}$ . Finally, multiple linear regression (MLR) was used to find the statistical relationship between  $T_{a,m}$  and  $T_{a,c}$ , and the SHP and  $g_{s,c}$ . Results showed that the macroscopic approach smooths the spatial variability of transpiration rates.  $T_{a,c}$  increased with the saturated water content,  $\theta_s$ , and the slope of the water retention curve,  $n$ , while  $T_{a,m}$  decreased with increasing  $\theta_s$  and  $n$ . MLR improved significantly by introducing  $g_{s,c}$  to predict  $T_{a,m}$ .

## Introduction

Actual transpiration by the plants,  $T_a$ , is a crucial component of the water balance. It involves stomatal diffusion of water taking place jointly with carbon dioxide exchange and is thus strictly connected to vegetation biomass yield. At the leaf scale, the transpiration process is controlled by the response of stomata to physiological and environmental factors such as irradiance, the temperature of the leaf, atmospheric water vapour pressure gradients, and CO<sub>2</sub> concentration (Buckley and Mott, 2002; Centritto *et al.*, 2011; Cowan and Farquhar, 1977). The single leaf transpiration may be measured by infrared gas analysers (IRGAs) designed explicitly for measuring CO<sub>2</sub> and H<sub>2</sub>O exchanges. In a single plant, sap flow measurements remain a reference tool for measuring transpiration (Marino *et al.*, 2014).

However, mathematical modelling can only evaluate the influence of the different environmental and physiological factors controlling transpiration at the canopy level. A crucial issue is developing a model that accounts for all the factors that control stomatal conductance.

Many models exist looking for a description of stomatal control of water and CO<sub>2</sub> fluxes at the leaf scale, some more focused on physiological aspects (for example, Leuning, 1995), some emphasising more the role of soil, plant, and atmospheric processes on water and CO<sub>2</sub> fluxes (Baldocchi and Meyers, 1998; Dewar, 2002; Williams *et al.*, 1996). For example, the response of stomatal conductance to environmental and physiological variables has been modelled by Jarvis *et al.* (1976) through a semi-empirical model relating stomatal conductance to irradiance, the temperature of the leaf, and soil water pressure head.

Relating leaf-to-canopy transpiration is not a simple task, as it generally involves scaling up leaf-scale stomatal conductance measurements to the canopy scale. While leaf stomatal conductance and other factors controlling evapotranspiration are relatively easy to measure, estimating canopy conductance requires complex mechanistic or empirical approaches (Jarvis and McNaughton,

Correspondence: Shawkat B.M. Hassan, School of Agricultural, Forestry, Food and Environmental Sciences (SAFE), University of Basilicata, via dell'Ateneo Lucano 10, 85100 Potenza, Italy.  
E-mail: shawkat.hassan@unibas.it

Key words: agro-hydrological modelling; canopy-scale transpiration; leaf-scale transpiration; soil hydraulic properties.

Acknowledgments: this work was performed thanks to the Eni S.p.A. (ENI)-CNR joint Research Institute on Water 'Hypatia of Alexandria' (Metaponto, Italy). ENI funded the Ph.D. grant of A.S.

Contributions: the authors contributed equally.

Conflict of interest: the authors declare no potential conflict of interest.

Received: 29 November 2022.

Accepted: 24 February 2023.

Early view: 20 June 2023.

©Copyright: the Author(s), 2023

Licensee PAGEPress, Italy

Journal of Agricultural Engineering 2023; LIV:1527

doi:10.4081/jae.2023.1527

This work is licensed under a Creative Commons Attribution-NonCommercial 4.0 International License (CC BY-NC 4.0).

Publisher's note: all claims expressed in this article are solely those of the authors and do not necessarily represent those of their affiliated organizations, or those of the publisher, the editors and the reviewers. Any product that may be evaluated in this article or claim that may be made by its manufacturer is not guaranteed or endorsed by the publisher.

1986; Shuttleworth, 2007). A common approach is the so-called ‘big-leaf’ model, where the canopy is considered a ‘macro-leaf’ whose conductance is obtained by scaling the leaf-scale stomatal conductance through a leaf area index (LAI) by accounting for an extinction factor. Another approach is the so-called dual-source model proposed by Shuttleworth and Wallace (1985), which separately estimates evaporation and transpiration and accounts for the biophysical and hydrological processes occurring within the canopy. However, the model involves complex parameterisation and has been primarily used in simplified versions, which limits the model’s strength (Brisson *et al.*, 1998; Li *et al.*, 2010).

The big-leaf assumption itself does not consider the complex structure of the canopy, where the leaf distribution, which affects the transpiration fluxes from the canopy, changes with canopy heights and leaf angles (Baldocchi and Meyers, 1998). Nevertheless, many studies have proven the practical validity of the big-leaf approach (Monteith and Unsworth, 2013; Mu *et al.*, 2011). The well-known and consolidated Penman-Monteith equation, estimating evapotranspiration (evaporation plus transpiration) at the canopy scale, is based on the big-leaf approach to calculate the canopy conductance ( $G_c$ ) required by the equation (Monteith and Unsworth, 2013).

Canopy-scale transpiration is an essential input for agro-hydrological models, which are increasingly used for applications at field or larger scales. The hydrological component of dynamics, physically based agro-hydrological models generally rely on mechanistic descriptions of water flow (and solute transport) in soils (Abrahamsen and Hansen, 2000; Comegna *et al.*, 2020; Coppola *et al.*, 2011, 2019; Šimůnek *et al.*, 2008; van Dam *et al.*, 1997). Richards’ equation (RE) is generally used for water flow and requires the soil water content-pressure head,  $q(h)$ , and hydraulic conductivity-water content,  $K(q)$ , functions as an input. Generally, RE has to be solved numerically by dividing the flow fields into several simulation compartments where the equation has to be solved with either finite differences or finite elements methods. Frequently, when these models have to be used at applicative scales (field-scale, for example), they use a macroscopic approach for root uptake so that potential transpiration,  $T_p$ , is distributed over the numerical simulation nodes in the whole root zone proportionally to root density (Feddes and Raats, 2004), to evaluate the potential water uptake in each node,  $S_p$ . To calculate the actual water uptake in each node,  $S_a$ ,  $S_p$  is eventually reduced in the case of water and salinity stresses, whose presence is evaluated based on soil water content and salinity in each simulation node (Molz, 1981).  $S_a$  is thus included in the RE as a so-called sink term. Integrating  $S_a$  over the root zone provides the  $T_a$  calculated by the model, hereafter  $T_{a,m}$ . The macroscopic approach does not describe the plant and its root system dynamically and in detail. It neglects the effects of the root geometry and flow pathways around roots. With this approach, the root system is rather modelled in a static way and represents a pump drawing water from different soil compartments according to a given root distribution,  $g(z)$ . The characteristics of the aerial part of the plant are generally given as LAI, and leaves distribution is just described through an extinction coefficient,  $k$ , for solar radiation within the canopy. The  $g(z)$ , LAI, and  $k$  must be provided as input to the model.

There are also microscopic approaches focusing on descriptions of radial flow to, and uptake by, individual roots and its transpiration through leaves stomata (Roose and Fowler, 2004; Schröder *et al.*, 2008). In any case, because of the complexity of the roots’ geometry and the flow equations into and through each rootlet, the application of the microscopic approach is still limited to the scale of a single plant and is not considered in this paper.

The macroscopic sink term’s variability results from the variability of the soil-water pressure and the osmotic potentials in the different simulation nodes in the root zone (Coppola *et al.*, 2015). Thus, as Coppola *et al.* (2015) discussed, the  $T_a$  calculated by a macroscopic approach in agro-hydrological models may be significantly impacted by the spatial and temporal variability of the water content (and salinity) in the root zone across a field. The water content variability in the root zone, in turn, is strictly related to the natural variability of the soil’s hydraulic properties. However, it is unclear to which extent the spatial variability of hydraulic properties also impacts the actual transpiration at the leaf scale.

Based on the premises above, there are plenty of approaches for measuring or estimating actual transpiration at different scales. However, there are some issues still deserving to be clarified, concerning: i) the relationship between actual transpiration measured at the microscopic leaf scale and that calculated by a macroscopic approach at the canopy scale; ii) the role of the spatial variability of soil hydraulic properties on both the leaf scale and canopy scale actual transpiration. To partially fill the gap, the purpose of this paper was to compare the actual transpiration, as measured at leaf scale and estimated by a macroscopic approach in an agro-hydrological model, under variable soil properties and water availability. For this purpose, sixteen plots were cultivated with tomato crops, of which eight were fully irrigated, and eight were irrigated under deficit irrigation (DI). The soil hydraulic parameters were obtained by a fast hydraulic characterisation method, hereafter called the TDR-2Dmod method (Coppola *et al.*, 2022). The LAI was obtained from each of the 16 plots using a leaf-area meter on six different days along the growth seasons. The microscopic transpiration rates, stomatal conductance, and photosynthesis were measured from single leaves of different plots using IRGAs, while the macroscopic transpiration fluxes were calculated for all sixteen plots using FLOWS physically-based agro-hydrological model (Coppola *et al.*, 2019). For the comparison, the  $T_a$  measured at leaf scale was first converted to canopy scale actual transpiration, hereafter  $T_{a,c}$ , using the big-leaf approach. Then, physical explanations were given for interpreting the behaviour observed in the  $T_{a,c}$  and that calculated by the macroscopic model,  $T_{a,m}$ . A multiple linear regression (MLR) was finally used to find the possibility of predicting  $T_{a,c}$  and  $T_{a,m}$  from the stomatal conductance and the soil hydraulic parameters.

## Materials and Methods

### Experimental field and setup

The experiment was carried out at the ‘Pantanello’ experimental farm (40°23’ N, 16°48’ E, altitude of 6 m a.s.l., and area  $\approx$  760 m<sup>2</sup>) in the Metaponto area (Southern Italy) from July to September 2020 (Figure 1).

A Mediterranean climate characterises the site according to the De Martonne classification. The texture of the first two soil horizons is classified as silty clay.

The study was conducted on two varieties of tomato, namely *Solanum lycopersicum*, cv. Impact F1 and cv. Contact F1 as described in Sillo *et al.* (2022). Tomatoes are the second most consumed vegetable crop worldwide (Frusciante *et al.*, 2000). It has high water demands due to the high  $ET_p$  rates and is reported to be sensitive to water deficits (Babalola and Fawusi, 1980; Rudich *et al.*, 1977).

The succession of operations generally involved deep plough-

ing (30 cm) and successive land milling. The transplant took place in July 2020 using seedlings of tomato with determined growth at the third fourth true leaf stage. The row distance was 1.0 m while the distance between plants on the rows was 0.30 m to obtain a density of 2.0 plants per  $m^2$ . Fertilisation was done with 120 kg/ha of  $P_2O_5$ , 150 kg/ha of  $K_2O$ , and 170 kg/ha of nitrogen.

The experimental site was subdivided into 16 plots of 18  $m^2$  (6m $\times$ 3m), divided into two groups of 8 plots, one irrigated with full irrigation (100% of the potential evapotranspiration,  $ET_p$ ) and one with DI (75% of  $ET_p$ ). Both tomato varieties were cultivated in each of the two groups of plots. This experimental scheme allowed exploring the dependence of transpiration fluxes on the variability of soil hydraulic properties also under deficit irrigation and different crop varieties. The two groups of plots were arranged according to a completely randomised design.

A dripper irrigation system applied irrigation. The irrigation system was carefully designed to guarantee more than 90% irrigation uniformity. All the plots were initially irrigated adequately until the plants were well established to avoid stress at early growth periods. During the whole growth season, 14 irrigations were made involving a total seasonal irrigation volume of 5.3  $m^3$  in control plots (100% irrigation) and 4.45  $m^3$  in water-stressed plots (75% irrigation). All the fruits were harvested by 5 September 2020.

### Meteorological data

Meteorological data came from a meteorological station installed very close to the experimental field. Data included: temperature, humidity, wind speed, and solar net radiation, which allowed calculating the reference evapotranspiration,  $ET_0$ , by the Penman-Monteith equation, in turn, converted to  $ET_p$  of tomato by using appropriate crop coefficients,  $K_c$ .

### Field measurements of soil hydraulic properties

Laboratory characterisation of the soil's hydraulic properties is a time-consuming and laborious process. There are other alternatives to overcome this problem, such as the indirect prediction of soil hydraulic properties from field infiltration measurements (e.g., Ankeny *et al.*, 1988; Šimůnek and van Genuchten, 1996) or by using pedotransfer functions (e.g., Arya and Paris 1981; Bouma, 1987; Hassan *et al.*, 2022). In this paper, a novel fast soil hydraulic characterisation method called the TDR-2Dmod method, was used, which integrates time domain reflectometry (TDR) measurements and 2D transient modelling of the water content dynamics in the wetted bulb developing in the soil under a point-source (Coppola *et al.*, 2022). TDR is a consolidated geophysical method for measuring soil water content and electrical conductivity in the same observation volume (Coppola *et al.*, 2016; Dragonetti *et al.*, 2018, 2022; Schaap *et al.*, 2003), which has recently been applied also to monitor immiscible contaminants in natural (Comegna *et al.*, 2013, 2016, 2017, 2019, 2022a) and artificial (Belviso *et al.*, 2022; Comegna *et al.*, 2022b) porous media. In practice, the method consists of irrigating the soil with a dripper (the point source) and monitoring the water content dynamics in the wetted bulb in soil under the dripper by one or more TDR probes (Figure 2). Inverse 2D modelling of these dynamics allows estimating the parameters of soil hydraulic properties under the dripper by using an optimisation algorithm that minimises an objective function, including the residuals between observed and simulated water contents. To this aim, the hydraulic functions are described by using parametric equations (Russo, 1988; van Genuchten, 1980).

Based on the monitoring of the evolution of the water bulb



**Figure 1.** A schematic view of the experimental design and a picture of the field at the harvesting time. Note the crop covering the plots completely.

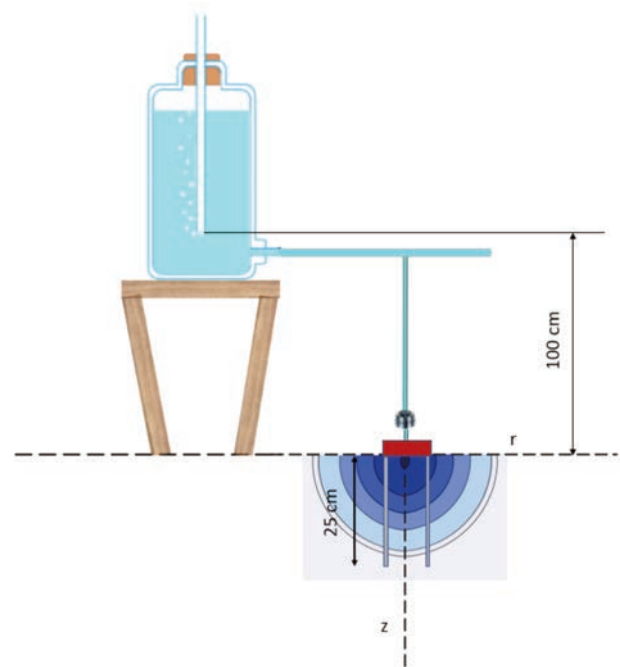


**Figure 2.** Experimental setup used for hydraulic characterisation by the TDR-2Dmod method (not to scale).

below a dripper, the method's strength is that it may be used for estimating the hydraulic properties in several sites simultaneously by a single field experiment involving irrigation of the field under study by a dripper system. The method describes the dynamics of the water inside the wetted bulb by the Warrick (1974) analytical solution of Richard's equation for flow from a point source (the dripper in our case) (for details on the Warrick analytical solution, see *Appendix*).

The soil hydraulic parameters ( $\alpha_{GR}$  and  $K_s$ ) used for linearising the Warrick (1974) analytical solution were determined as follows: In each of the 16 experimental plots, a 4 l/h, pressure-compensated dripper was used as a point source to irrigate the soil. The whole irrigation test lasted about 2 hours. The dripper, taken 5 cm from the soil surface, was connected to a Mariotte water reservoir with a bubbling point at 1 m from the dripper. A preliminary test was conducted to determine the dripper flow rate at a 1 m pressure head. On average, an actual flow rate of 3.7 l/h was measured and used as input for the simulations by the 2D model. During irrigation, the water content evolution in the wetting bulb was monitored using a two-wire probe, 25 cm length, 0.6 cm rod diameter, and 7 cm external rod spacing. The probe had an adapter (balun) to connect the coaxial cable to the two rods. The balun was immersed in the head of the probe, which was 8 cm wide, 4 cm in height, and 1.5 cm in thickness. The probe was embedded vertically below the dripper. To avoid interference with the dripping, the probe was installed with a very small insertion angle, as shown in (Figure 3b). During the infiltration experiment, the waveform was acquired at 2-minute intervals by using a TDR100 device (Campbell Scientific). Acquisition and subsequent interpretation of the TDR waveforms were performed through specifically developed software. Prior to installation, the probes were calibrated in the laboratory for water content measurements. The layout of the experimental setup is depicted in Figure 3.

All the data about the actual flow rate and the water contents measured by the TDR probe were used as input for a 2D modelling of the water distribution and dynamics in the wetted bulb based on the Warrick analytical solution for 2D flow from a point source. An inversion algorithm aiming at minimising the differences between the water contents measured by the TDR probe (hereafter  $q_{TDR}$ ) and the average water content predicted by the 2D model (hereafter  $q_{2D}$ ) in the same soil volume explored by the TDR probe allowed for optimising the parameters of the hydraulic properties in each of the irrigated sites. Appendix A details the water content calculation in the wetted bulb below a dripper using the Warrick (1974) analytical solution for 2D flow from a point source.

The parameters  $\alpha_{GRD}$ ,  $k$ , and  $K_s$  were considered fitting parameters. The parameters were estimated by solving an optimisation problem that minimises the deviations between the water content measured by the TDR probe (precisely, the average water content in the volume sampled by the TDR probe) and the average water content obtained by the 2D simulation in an observation volume comparable to that of TDR probe. The problem to be solved entails identifying the vector  $\mathbf{b}$  of the fitting parameters that minimises the following objective function:

$$O(\mathbf{b}) = \sum_{i=1}^N [\theta_{TDR}(t_i) - \theta_{2D}(t_i, \mathbf{b})]^2 \quad (1)$$

Involving the deviations between measured and simulated water contents at specified times  $t_i$  ( $i=1, 2, \dots, N$ ). Determination of  $\mathbf{b}$  was obtained by starting from an initial estimate of parameters  $b_i$ ,

using the optimisation algorithm of Levenberg-Marquardt. The method also supplies information on the uncertainty of estimated parameters, evaluating a first-order approximation of the covariance matrix of the parameters and calculating the confidence intervals of the individual parameters.

The appropriate evaluation of the volumes involved in the water content measurement by TDR is crucial for the comparison and that obtained by the 2D simulation of the flow field in the soil below the dripper. According to Topp and Ferré (2002), based on the calculations of the electrical field around the rods of a TDR probe proposed by Knight *et al.* (1995),  $\theta_{TDR}$  refers to an observation volume of the TDR probe which may be approximated by that of a cylinder of length equal to the length of the TDR rods (25 cm) and a diameter of about 1.5 times the outer rod spacing (10.5 cm). Thus, the volume explored by the TDR probe used in this study is approximately 2160 cm<sup>3</sup>. To make measurement and simulated volumes actually comparable,  $\theta_{2D}$  was obtained by averaging the simulated water contents in all the simulation nodes included in the volume explored by TDR. This may be seen in Figure 3, showing the simulation nodes (cross symbols) in a vertical section of the wetted bulb included in half of the TDR observation window (about 7 cm wide). Because of the radial symmetry of the simulated water content in the bulb, the water contents simulated on one half of the bulb are precisely the same in the other half. The same may be imagined for all the radial directions other than that shown in the figure. Thus, the average water content obtained in the planar window (half TDR section) shown in the figure corresponds to the average water content in the whole volume explored by the probe. Note in the figure that the calculation of the simulated average water content also includes a band of nodes a bit out of the

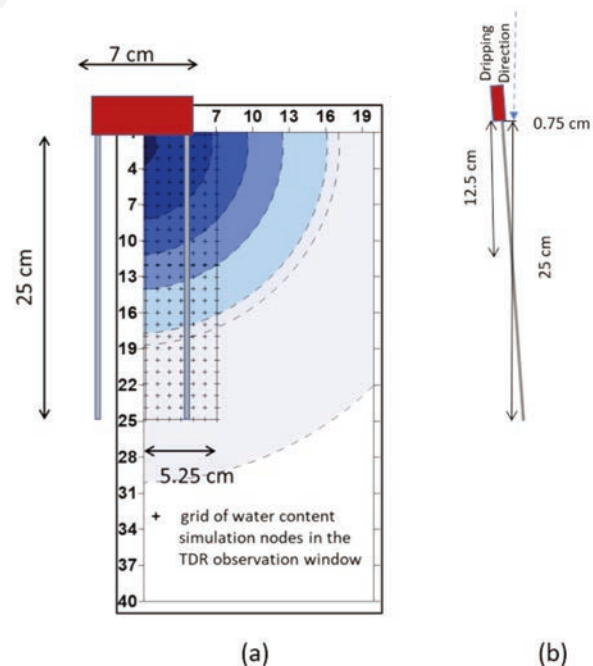


**Figure 3.** a) Schematic view of the portion of the 2D simulated flow field below the dripper used to calculate the average simulated water content to be compared to the measured one. The darker colour in the wetted bulb indicates higher water contents; b) Lateral view of the time domain reflectometry probe showing the small insertion angle to avoid interference with dripping.

TDR physical edge to account for the fact that the TDR probe explores a lateral size higher than the rods distance (about 1.5 times this distance). In other words, the average simulated water content was calculated on all the simulation nodes included in an area of 25 cm×5.25 cm. As the simulation was carried out by discretising the flow field in both depth and radial increments of 1 cm, the window considered for calculating the average simulated water content included six horizontal compartments and 25 vertical compartments for a total of 150 (25×6) nodes included in the calculation (excluding the nodes at  $r=0$  and  $z=0$ ).

Based on the procedure described above, the inversion forces the 2D model to provide water content (and pressure heads) in the TDR observation window comparable to those measured by TDR.

### Vegetation data

LAI, was needed to carry out the simulations by the macroscopic root uptake approach, and it is calculated as the ratio between the total leaf area to the ground area [ $\text{m}^2\text{m}^{-2}$ ]. LAI measurements were carried out using the leaf area meter (LI-3000, with conveyor belt assembly, LI-3050; Li-Cor, inc., Lincoln, NE, USA) on 19 May, 4 June, 19 June, 8 July, 6 August, and 10 August 2020 for all the 16 plots. The daily values of LAI were then obtained by linear interpolation using the 6 measured data points.

The crop coefficient,  $K_c$ , was obtained as a function of LAI using the logarithmic relationship in equation (1, which was empirically developed by Čereković *et al.* (2010) for tomato fields in southern Italy.

$$K_c = 0.2018 \ln(\text{LAI}) + 1.0926 \quad (2)$$

### Macroscopic root-water uptake calculation using agro-hydrological modelling

The agro-hydrological model utilised in this study is the FLOWS model (Coppola *et al.*, 2019). This model simulates the vertical transient flow in vegetated soils using the one-dimensional Richards equation [equation (3)]. The equation is solved using implicit finite differences with explicit linearisation similar to the SWAP model (Van Dam *et al.*, 1997).

$$C(h) \frac{\partial h}{\partial t} = \frac{\partial}{\partial z} \left( K(h) \frac{\partial h}{\partial z} - K(h) \right) - S_w(h) \quad (3)$$

where  $C(h)=d\theta/dh$  ( $\text{L}^{-1}$ ) is the soil water capacity,  $h$  (L) is the soil water pressure head,  $t$  (T) is time,  $z$  (L) is the vertical coordinate being positive upward,  $K(h)$  ( $\text{L T}^{-1}$ ) is the hydraulic conductivity and  $S_w(h)$  ( $\text{T}^{-1}$ ) is a sink term describing water uptake by plant roots.

Equation (3) requires the soil hydraulic parameters, *i.e.*, water retention and hydraulic conductivity parameters. In this study, the water retention properties were described (van Genuchten, 1980):

$$S_e = \frac{\theta - \theta_r}{\theta_s - \theta_r} = [1 + |\alpha_{VG} h|^n]^{-m} \quad \begin{array}{l} h < 0 \\ h = 0 \end{array} \quad (4)$$

$$\theta = \theta_s$$

where  $S_e$  is the effective saturation,  $h$  is the soil water potential,  $\theta$  is the soil water content,  $\theta_s$  is the water content at saturation, and  $\theta_r$  is the residual water content.  $\alpha_{VG}$  [ $\text{cm}^{-1}$ ],  $n$  and  $m = 1-1/n$  are shape parameters. This water retention model was applied to Mualem's model to obtain the relative hydraulic conductivity,  $K_r(S_e)$ :

$$K_r(S_e) = \frac{K(S_e)}{K_s} = S_e^\tau \left[ 1 - (1 - S_e^{1/m})^m \right]^2 \quad (5)$$

where  $K_r$  is the relative hydraulic conductivity,  $K_s$  is the saturated hydraulic conductivity, and  $\tau$  is a parameter to account for tortuosity.

Root-water uptake was calculated using Feddes-type macroscopic approach that calculates the actual sink term in equation (3) empirically using observed responses to water and osmotic potentials (Feddes, 1978; Feddes and Raats, 2004). This paper focuses on the water stress, and thus, the sink term in equation (3) becomes  $S_a(h)$  which depends on 1) the root density distribution function  $g(z)$  and 2) the activity at any depth in the root zone during the crop's growth season. A uniform root density distribution function was adopted (Feddes, 1978):

$$g(z) = \frac{1}{Dr} \quad (6)$$

where  $Dr$  is the root depth.

The potential root water uptake over the unit depth at any depth along the root zone,  $S_p$  ( $\text{T}^{-1}$ ), was calculated by distributing the potential transpiration,  $T_p$  ( $\text{L T}^{-1}$ ), over the root zone depth,  $Dr$  (L), in proportion to the root density distribution,  $g(z)$  (Feddes and Raats, 2004):

$$S_p(z) = g(z)T_p \quad (7)$$

Low water availability, *i.e.*, water stress, reduces the potential root water uptake. The reduction coefficient,  $\alpha_{rw}$ , is thus introduced to obtain the actual sink term under water stress:

$$S_a = \alpha_{rw}(h)S_p = \alpha_{rw}(h)g(z)T_p \quad (8)$$

The reduction coefficient,  $\alpha_{rw}$ , depends on the soil-water pressure head. Integrating the sink term,  $S_a$ , over the root depth obtains the actual transpiration,  $T_a$ . More information on the FLOWS model can be found in Coppola *et al.* (2019).

### Microscopic transpiration calculation using *in situ* leaf-scale measurements

Field measurements of stomatal conductance, transpiration, and photosynthesis were carried out using the CIRAS-3 system (PP Systems, 2017) twice: on 5 and 10 August 2020 for all 16 plots. CIRAS-3 refers to a combined infrared analysis system. The system pumps and samples fresh air into infrared gas analysers, and IRGAs. Figure 4 shows a schematic view of the IRGA system. Each IRGA consists of an infrared source, a known volume and length sample cell, an optical interference filter, and an infrared detector.

The infrared source produces light with mid-infrared wavelengths. The optical interference filter narrows the light bandwidth (*i.e.*, the range of light frequencies) to the signature wavelength, which is absorbed by gas molecules of interest (*i.e.*,  $\text{CO}_2$  or  $\text{H}_2\text{O}$ ). When the gas fills the sample cells, it absorbs the infrared light, IR, and the IR detector measures the reduction in IR strength is measured by the IR detector. According to Beer's law, this reduction can translate into the concentration of the gas of interest. Thus, the concentration of  $\text{CO}_2$  and  $\text{H}_2\text{O}$  can be measured using CIRAS-3 electronic processors by detecting the absorption of IR at the

wavelengths 4.26  $\mu\text{m}$  and 2.6  $\mu\text{m}$ , respectively. The flowmeter in CIRAS-3 measures the air volume flow rate ( $V_0$ ) in  $\text{cm}^3/\text{min}$  at standard temperature and pressure conditions (STP), i.e., at  $0^\circ\text{C}$  and 1013.25 mb. The ideal gas molar volume is 22.141 L/mol in STP. Therefore, the mass flow of air ( $W$ ) entering the cuvette in  $\text{mol m}^{-2} \text{s}^{-1}$  is:

$$W = \left(\frac{V_0}{60 \times 1000}\right) \times \left(\frac{1}{22.414}\right) \times \left(\frac{10^4}{a}\right) \quad (9)$$

where  $a$  is the projected leaf area in  $\text{cm}^2$ . The numbers in the equations are for unit conversions.

The transpiration rate can be calculated from the partial pressures of water vapour entering ( $e_{in}$ ) and exiting ( $e_{out}$ ) the cuvette. The water vapor's molar flow rate into the cuvette in  $\text{mol m}^2 \text{s}^{-1}$  is:

$$W_{\text{vapor},in} = W \times \left(\frac{e_{in}}{P}\right) \quad (10)$$

where  $P$  is the atmospheric pressure.

The airflow out of the cuvette is increased by the transpiration rate,  $T$ . Thus, the molar flow of water vapour out of the cuvette is:

$$W_{\text{vapor},out} = (W + T) \times \left(\frac{e_{out}}{P}\right) \quad (11)$$

Therefore, the transpiration rate in  $\text{mol m}^{-2} \text{s}^{-1}$  is the difference between the molar air flow into and out of the cuvette:

$$T = \left[ (W + T) \times \left(\frac{e_{out}}{P}\right) \right] - \left[ W \times \left(\frac{e_{in}}{P}\right) \right] \quad (12)$$

$$T = \left[ \frac{W \times (e_{out} - e_{in})}{(P - e_{out})} \right]$$

The difference between leaf and air temperatures,  $\Delta t$ , can be calculated as (Parkinson, 1983):

$$\Delta t = \left[ \frac{H - \lambda \times T}{\left(\frac{0.93 \times M_a \times C_p}{r_b}\right) + [4\sigma \times (t_c + 273)^3]} \right] \quad (13)$$

where  $H$  is the radiation absorbed by the leaf,  $\lambda$  is the latent heat by vaporisation of water,  $T$  is the transpiration rate,  $M_a$  is the air molecular weight,  $C_p$  is the specific heat at constant pressure,  $r_b$  is the boundary layer resistance to vapour transfer which is empirically determined for each cuvette using a filter paper,  $\sigma$  is the Stefan Boltzmann constant and  $t_c$  is the cuvette temperature.

The leaf temperature can then be calculated as follows:

$$t_{\text{leaf}} = t_c + \Delta t \quad (14)$$

The saturation vapour pressure,  $e_{\text{leaf}}$  can be calculated from  $t_{\text{leaf}}$  (Buck, 1981):

$$e_{\text{leaf}} = 6.1365 \times \exp\left(\frac{17.502 t_{\text{leaf}}}{240.97 + t_{\text{leaf}}}\right) \quad (15)$$

The total conductance,  $g_{\text{total}}$ , can be calculated using von Caemmerer and Farquhar (1981) model:

$$g_{\text{total}} = \frac{T \times \left(P - \frac{e_{\text{leaf}} + e_{\text{out}}}{2}\right)}{(e_{\text{leaf}} - e_{\text{out}})} \quad (16)$$

However, the total conductance is  $[1/(r_s+r_b)]$ , where  $r_s$  is the stomatal resistance and  $r_b$  is the boundary resistance. Therefore, the stomatal resistance,  $r_s$  in  $\text{m}^2 \text{s mol}^{-1}$  is:

$$r_s = \left[ \frac{e_{\text{leaf}} - e_{\text{out}}}{T \times \left(P - \frac{e_{\text{leaf}} + e_{\text{out}}}{2}\right)} \right] - r_b \quad (17)$$

And then, the stomatal conductance  $g_s$  can be calculated as  $(1/r_s)$ .

The net photosynthesis,  $A$ , can be calculated from the difference between  $\text{CO}_2$  concentrations entering ( $C_{in}$ ) and exiting ( $C_{out}$ ) the cuvette. The  $\text{CO}_2$  readings by IRGA are corrected for vapour pressure, temperature, and atmospheric pressure. The additional vapour from transpiration dilutes the  $C_{out}$  concentration. Thus, it is compensated as follows:

$$A = (C_{in} \times W) - C_{out} \times (W + T) \quad (18)$$

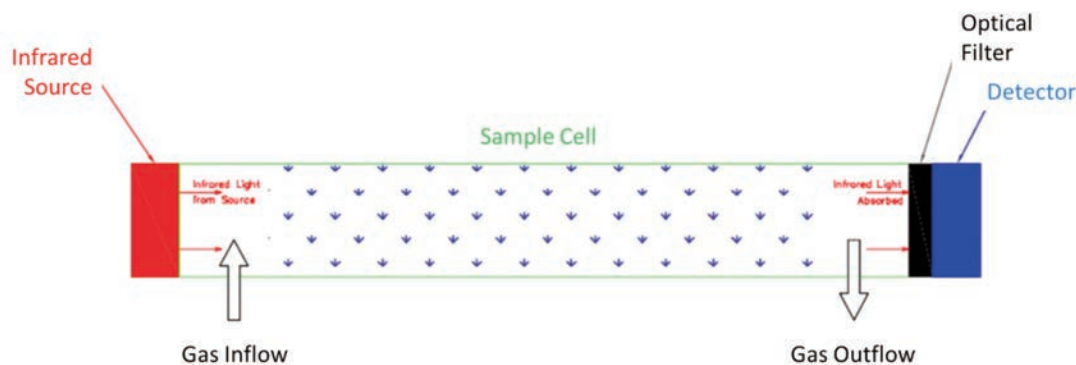


**Figure 4.** Schematic view of the infrared gas analysers system. Each infrared gas analysers consists of an infrared source, a known volume and length sample cell, an optical interference filter, and an infrared detector (adapted from PP Systems, 2017).

## Upscaling of transpiration and stomatal conductance from leaf scale to canopy scale

For the sake of comparison between the leaf-scale transpiration and that obtained from the FLOWS model, the leaf-scale stomatal conductance measured by the CIRAS-3 system,  $g_{s,l}$ , was upscaled to canopy-scale  $g_{s,c}$ , using the big-leaf approach. The big-leaf approach was carried out using Beer's law and an extinction factor,  $k$ , to account for the attenuation of the solar radiation in the canopy:

$$g_{s,c} = g_{s,l} \times \frac{1 - \exp(-k \times LAI)}{k} \quad (19)$$

where  $g_{s,c}$  is the canopy stomatal conductance, and  $g_{s,l}$  is the leaf-scale stomatal conductance. Then, the transpiration rates were calculated using the Penman-Monteith model and the canopy-scale stomatal conductance,  $g_{s,c}$ :

$$T_{a,c} = \frac{\Delta(R_n - G) + \rho C_p VPD}{\Delta + \left(1 + \frac{g_v}{g_{s,c}}\right) \gamma} \times \frac{1}{\lambda} \quad (20)$$

where  $T_{a,c}$  is the transpiration rate at canopy scale,  $D$  is the slope of the saturation vapour pressure curve at air temperature,  $R_n$  is the net solar radiation,  $G$  is the soil heat flux,  $\rho$  is the air density, VPD is the vapour pressure deficit,  $\gamma$  is the psychrometric constant,  $\lambda$  is the latent heat of evaporating water,  $g_v$  is the leaf boundary layer conductance for water vapour and  $g_{s,c}$  is the canopy-scale stomatal conductance.

Since the leaf-scale field measurements were carried out twice for each plot, the stomatal conductance and transpiration rates were averaged for each plot as follows: i) the average of the two field measurements for each plot (on 5 and 10 August 2020) and ii) the average of the daily transpiration rates calculated by FLOWS model between 20 July and 10 August 2020.

In order to find the statistical dependence of the canopy-level transpiration rates on the soil hydraulic parameters, multiple linear regression, MLR, was utilised to find the relationship between  $T_{a,c}$  and the soil hydraulic parameters and  $g_{s,c}$ . MLR was also applied to the transpiration rates obtained from the FLOWS model,  $T_{a,m}$ , to find its statistical dependence on the same parameters. Before carrying out MLR, the soil hydraulic parameters and  $g_{s,c}$  were nor-

malised by dividing each parameter by its mean value. The purpose of normalisation by dividing each parameter by its mean value is to facilitate the interpretation of the MLR results since the parameters used in MLR had different scales. Normalising each parameter before applying MLR made the coefficients more representative of the statistical dependence of  $T_{a,c}$  and  $T_{a,m}$  on soil hydraulic parameters and  $g_{s,c}$ .

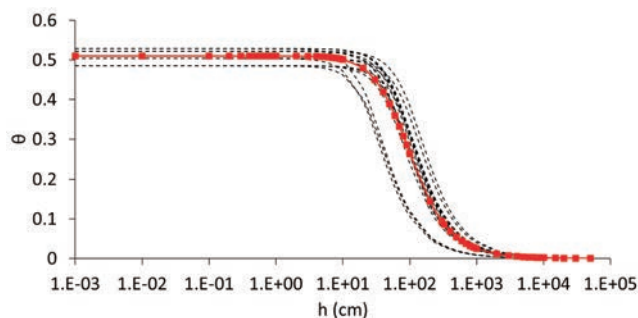
## Results and Discussion

### Hydraulic properties and their spatial variability

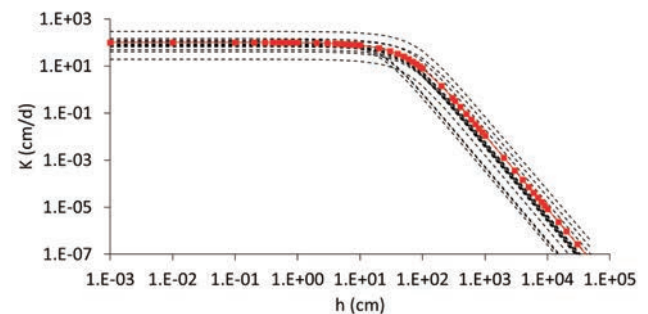
Figure 5 shows the Water Retention Curves (WRC) of all 16 plots (black dashed lines) and the average WRC obtained as the average water content at each soil water pressure (red solid lines with markers). Figure 6 shows the Hydraulic Conductivity Curves (HCC) of all 16 plots (black dashed lines) and the average HCC obtained as the average hydraulic conductivity at each soil water pressure (red solid lines with markers). Figures 5 and 6 show that, even in a small experimental area, there is a noticeable spatial variability of soil hydraulic properties. As expected, this variability is more apparent in the air entry potentials ( $1/\alpha_{vG}$ ) and  $K_s$  parameters, frequently observed in homogeneous and layered soils (Severino and Coppola, 2013) and affects the root water uptake significantly. This will be clearer later.

Table 1 reports the soil hydraulic parameter values for all 16 plots and their averages and standard deviations. The table shows that plot R1-4 had a particularly low saturated hydraulic conductivity,  $K_s$ , with a value of 18.974 cm/d compared to the average of 99.86 cm/d.

Figure 7 shows the colour-graduated maps of the canopy transpiration rates,  $T_{a,c}$ , obtained as upscaled leaf-scale transpiration on the left and of the macroscopic transpiration rates obtained from the FLOWS model,  $T_{a,m}$ , on the right. The canopy transpiration rates in the map represent the averages of two measurements carried out on 5 and 10 August 2020. Accordingly, the model macroscopic transpiration rates were obtained as averages of daily transpiration rates simulated between 5 and 10 August 2020. The figure shows that the spatial variability of the canopy-scale transpiration is significantly higher than that of the transpiration obtained by the macroscopic approach using FLOWS agro-hydrological model.



**Figure 5.** The water retention curves, for all the 16 plots (black dashed lines). The red solid line with symbols represents the average water retention curves obtained as the average water content at each soil water pressure.



**Figure 6.** The hydraulic conductivity curves of all 16 plots (black dashed lines). The red line with the symbols represents the average hydraulic conductivity curves obtained as the average hydraulic conductivity at each soil water pressure.

Figure 8 shows the maps of the soil hydraulic property parameters. The upper left map represents saturated water content,  $\theta_s$ , the upper right map represents the parameter  $\alpha_{vG}$ , the lower left map represents the parameter  $n_{vG}$  and the lower right map represents the saturated hydraulic conductivity,  $K_s$ . Table 1 and Figure 8 show that the spatial variability of soil hydraulic parameters in the study area is especially apparent for the saturated hydraulic conductivity. In any case, the parameter  $\alpha_{vG}$  varies in the range 0.01-0.03, which may significantly affect the simulations for high water contents. The parameter  $n_{vG}$  has an average value of 2.384 (Table 1), indicating a relatively permeable porous system, which was not expected for a silty-clay texture. In any case, this behaviour can be explained by the fact that the soil is quite well structured, as also suggested by the quite high values of the  $K_s$ .

## Transpiration rates

Figure 9 shows the leaf-scale transpiration rates,  $T_{a,l}$  (black columns), the canopy-scale transpiration rates,  $T_{a,c}$  (blue columns) obtained by the previous one through the big-leaf approach, and the macroscopic transpiration rates calculated by FLOWS,  $T_{a,m}$ , agro-hydrological model (orange columns) for the 16 plots. Plot labels starting with R1 refer to the plots irrigated with 100% of ET, while those starting with R2 refer to the plots with deficit irrigation. The mean values for  $T_{a,c}$  and  $T_{a,m}$  were 0.46 and 0.38 cm/day, respectively, and the standard deviations were 0.09 and 0.17 cm/day, respectively. The  $T_{a,l}$  and, subsequently,  $T_{a,c}$  had higher spatial variabilities than  $T_{a,m}$  because the leaf-scale measurements are affected by the variability and the diversity of the leaves within each plot; transpiration rates from different leaves are variable



**Figure 7.** Colour-graduated maps of the canopy transpiration rates,  $T_{a,c}$ , obtained as upscaled leaf-scale transpiration on the left and of the macroscopic transpiration rates obtained from FLOWS model,  $T_{a,m}$ , on the right. The canopy transpiration rates in the maps represent the averages of two daily transpiration rate measurements carried out on 5 and 10 August 2020.

**Table 1.** The soil hydraulic parameter values for all 16 plots, as well as their averages and standard deviations.

Plot	$r_b$ (g m <sup>-3</sup> )	$q_s$ (m <sup>3</sup> m <sup>-3</sup> )	$\alpha$	$n$	$K_s$ (cm/day)
R1-1	1.364	0.485	0.034	2.579	111.348
R1-2	1.267	0.522	0.009	2.259	121.812
R1-3	1.314	0.504	0.010	2.116	293.558
R1-4	1.248	0.529	0.013	2.366	18.974
R1-5	1.364	0.485	0.013	2.539	78.111
R1-6	1.267	0.522	0.016	2.651	104.349
R1-7	1.314	0.504	0.039	2.190	111.480
R1-8	1.248	0.529	0.013	2.506	48.682
R2-1	1.364	0.485	0.011	2.437	143.994
R2-2	1.267	0.522	0.016	2.472	84.550
R2-3	1.314	0.504	0.012	2.226	87.879
R2-4	1.248	0.529	0.036	2.295	142.719
R2-5	1.364	0.485	0.016	2.616	74.020
R2-6	1.267	0.522	0.014	2.157	69.570
R2-7	1.248	0.529	0.012	2.330	40.364
R2-8	1.314	0.504	0.015	2.403	66.414
Average	1.299	0.510	0.017	2.384	99.864
Standard deviation	0.046	0.017	0.010	0.168	62.359

depending on the leaf size, water-stress status within the leaves and the canopy structure. The lower variability of the  $T_{a,m}$  indicates that the agro-hydrological model smooths the transpiration rate variability. In a sense, the model produces a sort of filtering of the small-scale (high frequency) variability. This is desirable from a management point of view, as the quite erratic values coming from small-scale measurements would introduce uncertainties in evaluating the actual transpiration rate. As for the  $T_{a,l}$  and  $T_{a,c}$ , the R1

transpiration rates are, on average higher than the R2 plots but with a much larger variability, such that in some cases, the R1 transpiration rate is either similar or even lower than that observed in the R2 plots. The  $T_{a,m}$  values confirm the average behaviour observed in the  $T_{a,l}$  and  $T_{a,c}$  cases. Only in one case (plot R1-4) the transpiration rate simulated for the 100% irrigation volume produces a stress similar to that simulated for the 75% irrigation volume.

Compared to the direct measurements, which can be carried

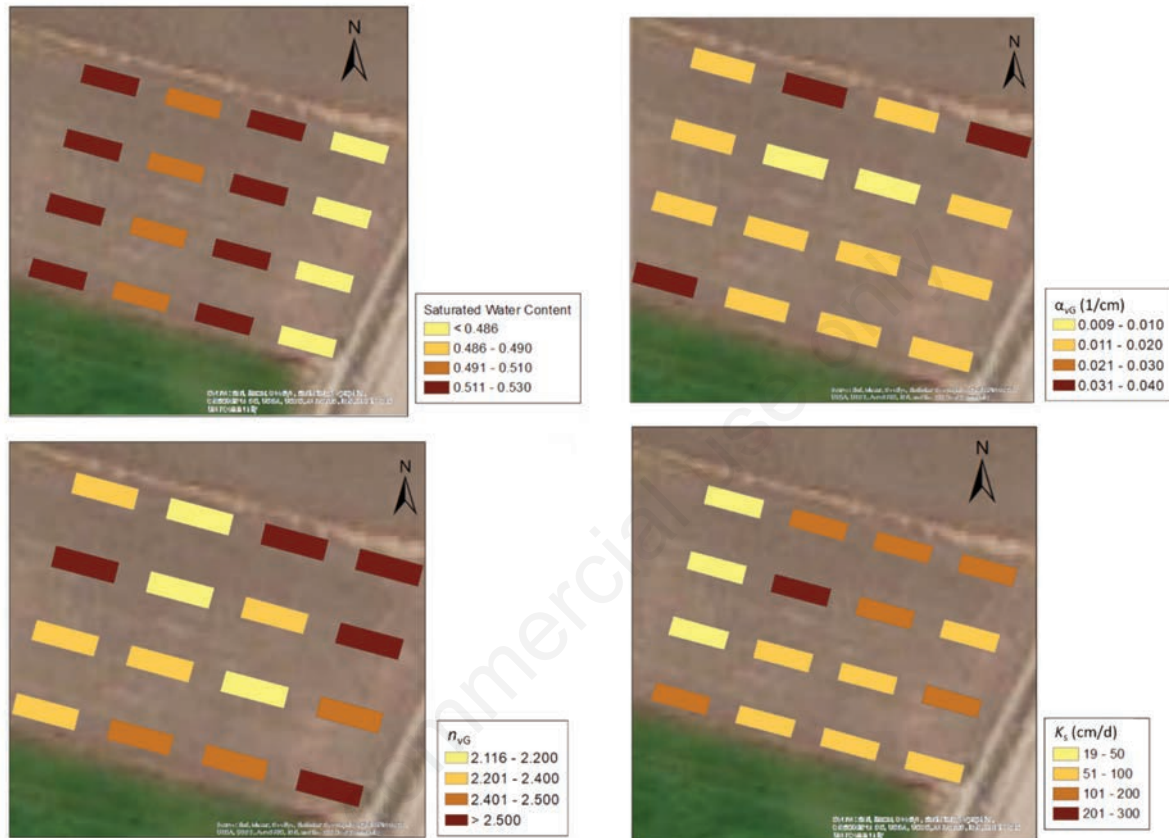


**Figure 8.** Colour-graduated maps of the soil hydraulic property parameters. The upper left map represents saturated water content,  $\theta_s$ , the upper right map represents the parameter  $\alpha_{vG}$ , the lower left map represents the parameter  $n_{vG}$  and the lower right map represents the saturated hydraulic conductivity,  $K_s$ .

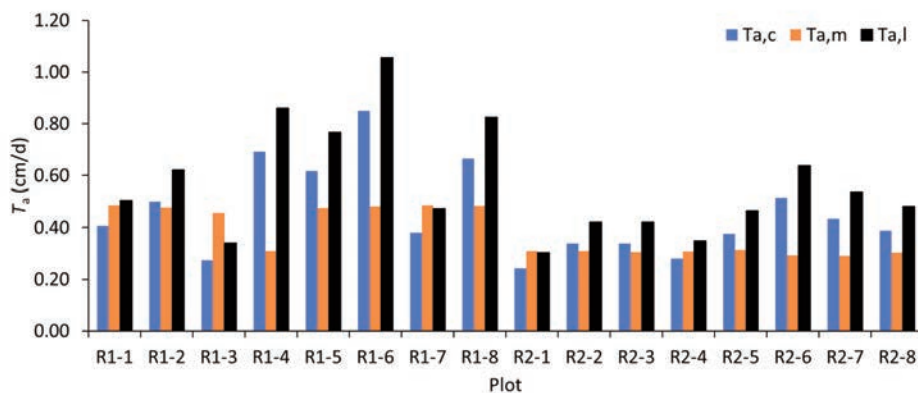


**Figure 9.** CLeaf-scale transpiration rates (black columns),  $T_{a,l}$ , canopy-scale transpiration rates (blue columns),  $T_{a,c}$ , and the transpiration rates calculated by FLOWS agro-hydrological model (orange columns),  $T_{a,m}$ , for the 16 plots. Plot names starting with R1 refer to the control plots, while those starting with R2 refer to the plots with deficit irrigation.

out only a limited number of times, the strength of the agro-hydrological model lies in the fact that, once adequately calibrated, it allows for estimating the transpiration fluxes over the whole growth season of the crop. The daily ratios between the cumulative actual transpiration rates obtained using the macroscopic approach,  $T_{a,m}$ , and the cumulative potential transpiration rates,  $T_p$ , in all 16 plots are shown in Figure 10. Figure 10 shows that, generally, the R1 group's ratio of cumulative ( $T_{a,m} / T_p$ ) was close to 1.00 except for plot R1-4, whose ratio was below 0.80, similar to the R2 group. Plot R1-4, in fact, experienced water stress, although it was supplied with irrigation of 100% of  $ET_p$ . However, the water stress in plot R1-4 stems from the site-specific soil hydrological behaviour, which depends on the soil hydraulic properties, rather than the quantity of applied irrigation water.

Using the agro-hydrological model to obtain the root water uptake and, subsequently, the transpiration rates (*i.e.*, the macroscopic approach) provided information about the temporal vari-

ability of transpiration rates along all growth seasons as shown in Figure 10. On the other hand, this information is more complicated to obtain using the microscopic approach as it requires extensive field measurements rather than mathematical models.

### Relationship between canopy-level transpiration rates and the soil hydraulic parameters

Figure 11 shows the  $T_{a,c}$  rates predicted by MLR plotted against the  $T_{a,c}$  rates obtained by upscaling the leaf-scale transpiration rates. The root-mean-square error, RMSE, was 0.12 cm/d. The coefficient of correlation,  $R$ , was 0.67. The second column in Table 2 shows the intercept and the coefficients of the normalised hydraulic parameters used in the MLR to predict the  $T_{a,c}$  rates. Before carrying out the MLR analysis, the parameters were normalised by dividing each parameter by its mean value. The table indicates that the parameters  $n$  and  $\theta_s$  significantly affect the upscaled, canopy-scale transpiration rates.

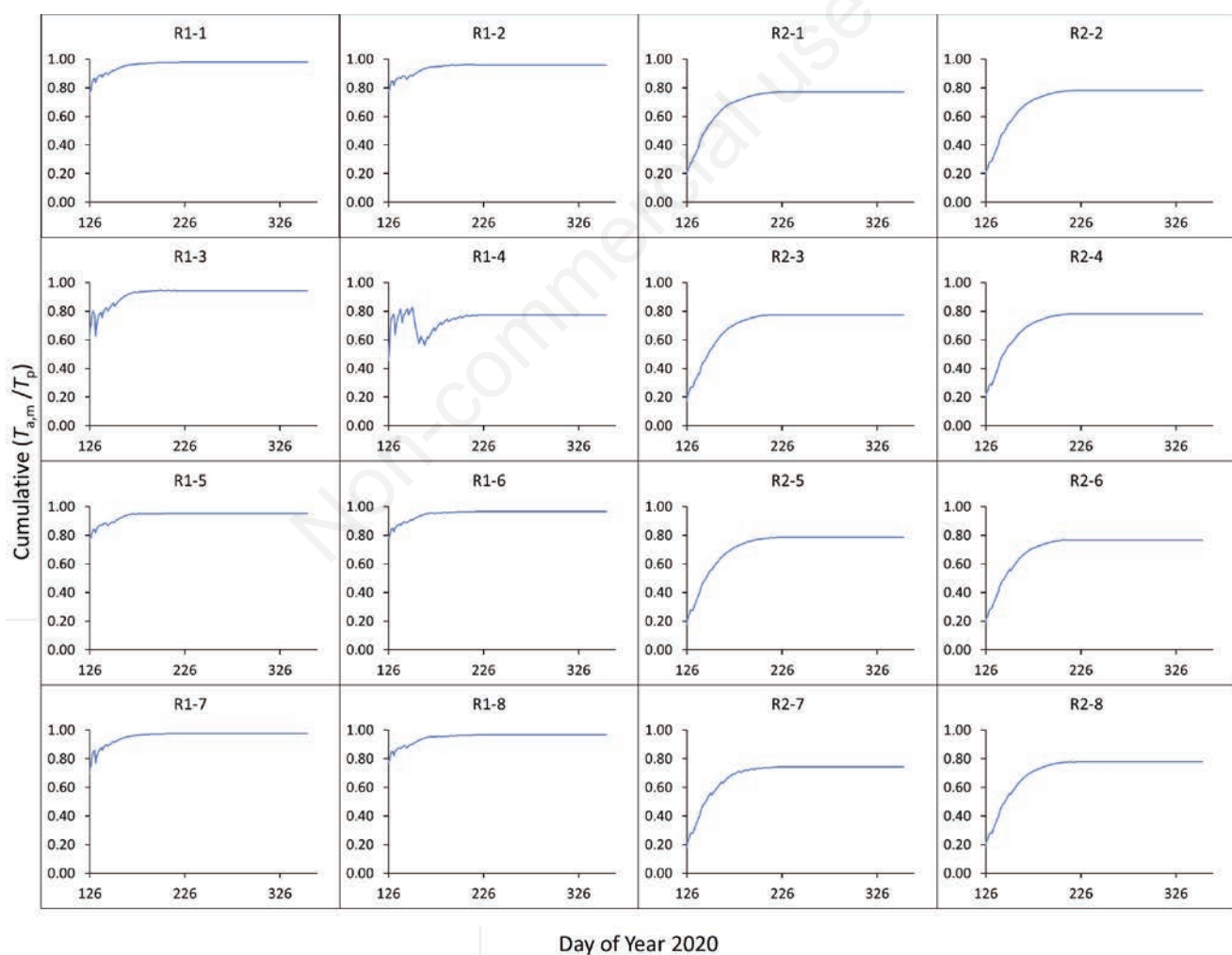


**Figure 10.** The daily ratio between cumulative actual transpiration rates obtained using the macroscopic approach,  $T_{a,m}$ , and the cumulative potential transpiration rates,  $T_p$ , for all the 16 plots in the study area

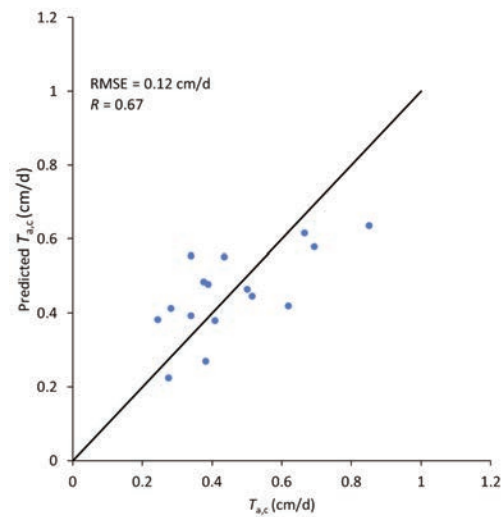
### Relationship between transpiration rates obtained by FLOWS, the soil hydraulic parameters, and the canopy-scale stomatal conductance

Figure 12 shows the  $T_{a,m}$  rates predicted by MLR against the  $T_{a,m}$  rates obtained by FLOWS, MLR, using: a) the normalised SHP (on the left), and b) using the normalised SHP and the normalised canopy-scale stomatal conductance,  $g_{s,c}$  (on the right). The root-mean-square errors, RMSE, were 0.08 cm/d and 0.05 cm/d for case (a) and case (b), respectively. The coefficients of correlation,  $R$ , were 0.43 and 0.79, respectively.

The low  $R$ -value in Figure 12a indicates that the soil hydraulic parameters do not contain enough information to predict the transpiration rates obtained from agro-hydrological modelling. Figure 12b, on the other hand, indicates that including  $g_{s,c}$  into MLR improves its ability to predict  $T_{a,m}$  rates with an  $R$ -value of 0.79.

Both cases (a) and (b) in Table 2 indicate that the parameters  $n_{VG}$  and  $\theta_s$  significantly affect the  $T_{a,m}$  rates obtained by the macroscopic model. However, after improving the MLR by including  $g_{s,c}$ , table 2 shows that the macroscopic transpiration rates obtained using agro-hydrological modelling focused on soil-water processes are inversely proportional to the parameters  $\theta_s$  and  $n_{VG}$ .

Looking at Figure 12b, there are two clusters of values: i) the values to the lower left representing the plots with DI as well as the



**Figure 11.** The  $T_{a,c}$  rates predicted by multiple linear regression using the normalised soil hydraulic parameters, plotted against the  $T_{a,c}$  rates obtained by upscaling the leaf-scale transpiration rates. The figure also reports the root mean square error and the correlation coefficient,  $R$ .

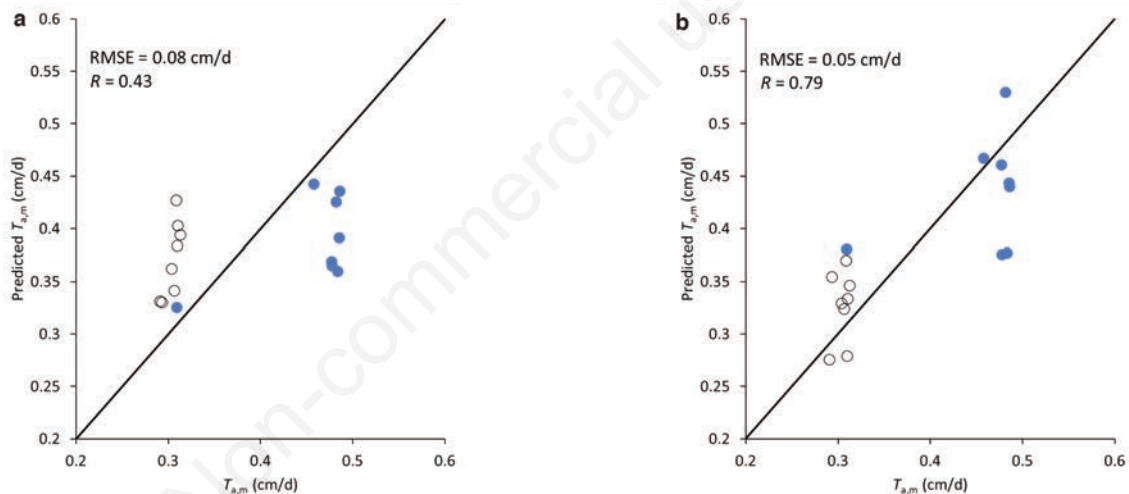


**Figure 12.** The  $T_{a,m}$  rates predicted by multiple linear regression plotted against the  $T_{a,m}$  rates obtained by FLOWS using: a) the normalised soil hydraulic parameters (on the left), and b) using the normalised soil hydraulic parameters and the normalised canopy-scale stomatal conductance,  $g_{s,c}$  (on the right). The figure also reports the root mean square error and the correlation coefficient,  $R$ . The blue circle markers represent the control group (R1 plots), and the black markers represent the group with deficit irrigation (R2 plots).

**Table 2.** The multiple linear regression intercepts and coefficients of the normalised soil hydraulic parameters, and canopy-scale stomatal conductance,  $g_{s,c}$ , to obtain the canopy-scale transpiration rates,  $T_{a,c}$ , and the transpiration rates obtained by FLOWS model,  $T_{a,m}$ .

Normalised parameter	Coefficients		
	$T_{a,c}$ *	$T_{a,m}$ (a)**	$T_{a,m}$ (b)***
Intercept	-18.93	-5.59	3.18
$\theta_s$	2.15	0.13	-0.78
$\alpha$	-0.06	0.03	0.06
$n$	17.34	5.75	-2.36
$K_s$ (cm/day)	-0.04	0.06	0.08
$g_{s,c}$ (mmol/m <sup>2</sup> s)	-	-	0.20

\*The MLR intercept and coefficients to obtain  $T_{a,c}$  from the SHP; \*\*The MLR intercept and coefficients to obtain  $T_{a,m}$  from the SHP; \*\*\*The MLR intercept and coefficients to obtain  $T_{a,m}$  from the SHP and  $g_{s,c}$ ; MLR, multiple linear regression; SHP, soil hydraulic parameters.

plot R1-4, and ii) the values to the upper right representing the plots with full irrigation except plot R1-4. The relatively lower R1-4 transpiration rates can be explained by its hydraulic properties (Table 1); plot R1-4 had the lowest value for  $K_s$  of 18.974 cm/d. The low conductivity in R1-4 led to the accumulation of water storage in the root zone, causing soil-water pressure head values to exceed the field capacity and to frequently reach saturation. The high pressure-head values reduce the water stress coefficient (*i.e.*,  $\alpha_{rw}$  in equation 8) due to oxygen deficit in the root zone. Figure 13 consists of two parts: (a) the upper part is the evolution of the average soil-water pressure head in the root zone obtained by the FLOWS model for the plots R1-1 (solid line) and R1-4 (dashed line) during the growth season, and (b) the lower part is the Feddes (1978) water stress response function used in this paper. The figure focuses on plot R1-4 because it experienced water stress, although it was supplied with 100% of  $ET_p$ , and compared plot R1-4 to plot R1-1, which did not experience stress. When the soil-water pressure head is above -1 cm, the stress coefficient,  $\alpha_{rw}$ , decreases due to oxygen deficit. Figure 13 shows that plot R1-4 experienced water stress caused by oxygen deficit compared to plot R1-1 in which the soil had a higher  $K_s$  value of 111.348 cm/d allowing for excess water drainage. This explains that plot's relatively low average transpiration rate, close to the transpiration rate values for R2 plots (the ones with DI) despite the higher  $g_{s,c}$  values for R1-4.

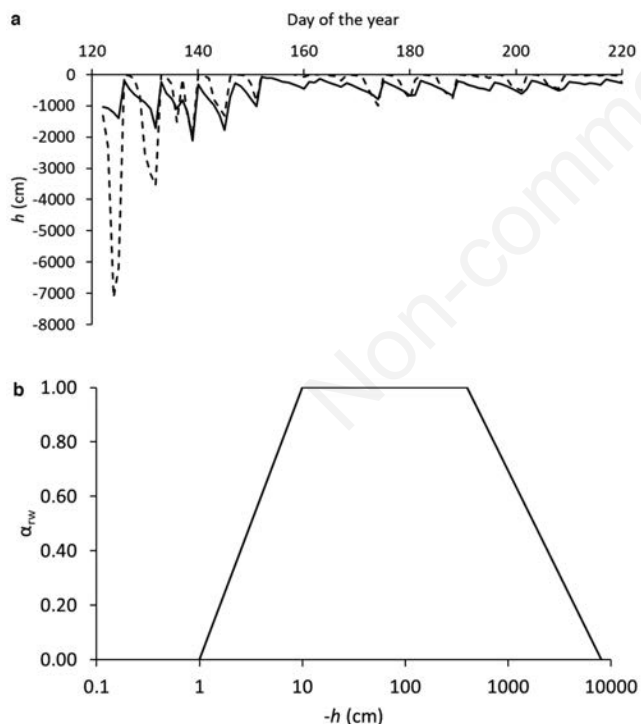


**Figure 13.** The upper part (a) is the evolution of the average soil-water pressure head in the root zone obtained by the FLOWS model for plots R1-1 (solid line) and R1-4 (dashed line) during the growth season. The lower part (b) is the Feddes (1978) water stress response function used in this paper; when the soil-water pressure head is above -1 cm, the stress coefficient,  $\alpha_{rw}$ , decreases due to oxygen deficit.

## Conclusions

The primary purpose of this paper was to find the relationship between the actual transpiration rates as measured at a microscopic leaf scale and as calculated by an agro-hydrological model at a macroscopic scale. The paper also aimed to find the relationship between actual transpiration rates and the variability of soil properties and irrigation techniques, *i.e.*, full irrigation and deficit irrigation. Soil hydraulic properties were obtained using a simple method called TDR2D-mod which integrates TDR measurements and 2D transient modelling of the water content dynamics in the wetted bulb developing in the soil under a point source. LAI was measured in the field, and the crop coefficient,  $K_c$ , was obtained from LAI using a previously developed empirical equation for tomato crops in southern Italy. Both the soil and vegetation properties were used as inputs in the physically-based agro-hydrological model, FLOWS, to estimate the actual root water uptake. The macroscopic actual transpiration was then obtained by integrating the root water uptake along the root zone. The microscopic leaf-scale transpiration rates and the stomatal conductance were measured in the field on two days at the end of the growth season, 5 and 10 August 2020, using IRGAs. For the sake of comparison with the macroscopic approach, the leaf-scale stomatal conductance,  $g_{s,l}$ , was upscaled to the canopy scale using the big-leaf approach obtaining the canopy-scale stomatal conductance,  $g_{s,c}$ . The latter was then introduced to the Penman-Monteith model to obtain the canopy-scale transpiration rates that were compared to the macroscopic transpiration rates.

The results showed that the transpiration rates obtained from FLOWS agro-hydrological model had lower variability than the canopy-scale transpiration rates obtained by upscaling the leaf-scale transpiration measurements. The agro-hydrological model smoothed the variability of the canopy-scale transpiration. The results also showed that the canopy-scale transpiration rates were proportional to the saturated water content and the parameter  $n$  in the van Genuchten water retention model in MLR. Using the soil hydraulic parameters to predict the transpiration rates obtained from the FLOWS agro-hydrological model by means of MLR was insufficient, with a relatively small coefficient of determination ( $R^2=0.19$ ). However, including the canopy-scale stomatal conductance,  $g_{s,c}$ , improved the MLR results, and it showed that increasing the values of  $\theta_s$  and  $n$  decreased the transpiration rates while increasing  $g_{s,c}$  increased the transpiration rates.

Upscaling the microscopic, leaf-scale transpiration rates to canopy scale differs in variability and statistical dependence from the transpiration rates obtained by agro-hydrological models focused on the soil processes. Also, the soil hydraulic properties are more effective in the root-water uptake than the stomatal conductance which is shown in the MLR results.

## References

- Abrahamsen P., Hansen S. 2000. Daisy: an open soil-crop-atmosphere system model. *Environ. Modell. Softw.* 15:313-30.
- Ankeny M.D., Kaspar T.C., Horton R. 1988. Design for an automated tension infiltrometer. *Soil Sci. Soc. Am. J.* 52:893-6.
- Arya L.M., Paris J.F. 1981. A physicoempirical model to predict the soil moisture characteristic from particle-size distribution and bulk density data. *Soil Sci. Soc. Am. J.* 45:1023-30.
- Babalola O., Fawusi M.O.A. 1980. Drought susceptibility of two tomato (*Lycopersicon esculentum*) varieties. *Plant Soil.*

- 55:205-14.
- Baldocchi D., Meyers T. 1998. On using eco-physiological, micrometeorological and biogeochemical theory to evaluate carbon dioxide, water vapor and trace gas fluxes over vegetation: a perspective. *Agr. Forest. Meteorol.* 90:1-25.
- Belviso C., Satriani A., Lovelli S., Comegna A., Coppola A., Dragonetti G., Cavalcante F., Rivelli A.R. 2022. Impact of zeolite from coal fly ash on soil hydrophysical properties and plant growth. *Agriculture.* 12:356.
- Bouma J. 1987. Transfer functions and threshold values: from soil characteristics to land qualities. Workshop on Quantified Land Evaluation Process. International Institute for Aerospace Survey and Earth Science, Washington, D.C., USA, 6:106-10.
- Brisson N., Itier B., L'Hotel J.C., Lorendeau J.Y. 1998. Parameterisation of the Shuttleworth-Wallace model to estimate daily maximum transpiration for use in crop models. *Ecol. Model.* 107:159-69.
- Buck A.L. 1981. New equations for computing vapor pressure and enhancement factor. *J. Appl. Meteorol. Clim.* 20:1527-32.
- Buckley T.N., Mott K.A. 2002. Dynamics of stomatal water relations during the humidity response: implications of two hypothetical mechanisms. *Plant Cell Environ.* 25:407-19.
- Centritto M., Tognetti R., Leitgeb E., Štřelcová K., Cohen S. 2011. Above ground processes: Anticipating climate change influences. In: Bredemeier M., Cohen S., Godbold D.L., Lode E., Pichler V., Schleppi P. (Eds.) *Forest management and the water cycle: An ecosystem-based approach*, Springer Dordrecht, Berlin, Germany, 31-64.
- Čerčević N., Todorović M., Snyder R.L. 2010. The relationship between leaf area index and crop coefficient for tomato crop grown in Southern Italy. *Euroinven.* 1:3-10.
- Comegna A., Coppola A., Dragonetti G. 2019. A soil non-aqueous phase liquid (NAPL) flushing laboratory experiment based on measuring the dielectric properties of soil-organic mixtures via time domain reflectometry (TDR). *Hydrol. Earth Syst. Sci.* 23:3593-602.
- Comegna A., Coppola A., Dragonetti G. 2020. Time domain reflectometry for dielectric characterization of olive mill wastewater contaminated soils. *J. Agr. Eng.* 51:248-54.
- Comegna A., Coppola A., Dragonetti G., Severino G., Sommella A., Basile A. 2013. Dielectric properties of a tilled sandy volcanic-vesuvian soil with moderate andic features. *Soil Till. Res.* 133:93-100.
- Comegna A., Coppola A., Dragonetti G., Sommella A. 2016. Estimating non-aqueous phase liquid content in variably saturated soils using time domain reflectometry. *Vadose Zone J.* 15:1-11.
- Comegna A., Coppola A., Dragonetti G., Sommella A. 2017. Interpreting TDR signal propagation through soils with distinct layers of nonaqueous-phase liquid and water content. *Vadose Zone J.* 16:1-11.
- Comegna A., Dragonetti G., Kodesova R., Coppola A., 2022b. Impact of olive mill wastewater (OMW) on the soil hydraulic and solute transport properties. *Int. J. Environ. Sci. Te.* 19:7079-92.
- Comegna A., Severino G., Coppola A., 2022a. A review of new TDR applications for measuring non-aqueous phase liquids (NAPLs) in soils. *Environ. Adv.* 9:100296.
- Coppola A., Chaali N., Dragonetti G., Lamaddalena N., Comegna A. 2015. Root uptake under non-uniform root-zone salinity. *Ecohydrology.* 8:1363-79.
- Coppola A., Comegna A., Dragonetti G., Dyck M., Basile A., Lamaddalena N., Kassab M., Comegna V. 2011. Solute transport scales in an unsaturated stony soil. *Adv. Water Resour.* 34:747-59.
- Coppola A., Dragonetti G., Moghrani S., Hassan S.B.M., Comegna A., 2022. A fast and simple method to measure soil hydraulic properties in multiple sites. Submitted to *Vadose Zone J.*
- Coppola A., Dragonetti G., Sengouga A., Lamaddalena N., Comegna A., Basile A., Noviello N., Nardella L. 2019. Identifying optimal irrigation water needs at district scale by using a physically based agro-hydrological model. *Water.* 11:841-65.
- Coppola A., Smettem K., Ajeel A., Saeed A., Dragonetti G., Comegna A., Lamaddalena N., Vacca A. 2016. Calibration of an electromagnetic induction sensor with time-domain reflectometry data to monitor rootzone electrical conductivity under saline water irrigation. *Eur. J. Soil Sci.* 67:737-48.
- Cowan I.R., Farquhar G.D. 1977. Stomatal function in relation to leaf metabolism and environment. *Sym. Soc. Exp. Biol.* 31:471-505.
- Dewar R.C. 2002. The Ball-Berry-Leuning and Tardieu-Davies stomatal models: synthesis and extension within a spatially aggregated picture of guard cell function. *Plant Cell Environ.* 25:1383-98.
- Dragonetti G., Comegna A., Ajeel A., Deidda G.P., Lamaddalena N., Rodriguez G., Vignoli G., Coppola A. 2018. Calibrating electromagnetic induction conductivities with time domain reflectometry measurements. *Hydrol. Earth Syst. Sci.* 22:1509-23.
- Dragonetti G., Farzamian M., Basile A., Santos F.M., Coppola A. 2022. In situ estimation of soil hydraulic and hydrodispersive properties by inversion of electromagnetic induction measurements and soil hydrological modeling. *Hydrol. Earth Syst. Sci.* 26:5119-36.
- Feddes R.A. 1978. *Simulation of field water use and crop yield.* PUDOC, Wageningen, The Netherlands, pp 189.
- Feddes R.A., Raats P.A.C. 2004. Parameterizing the soil-water-plant root system. In: Feddes R. A., de Rooij G. H., van Dam J. C. (Eds.) *Unsaturated-zone modeling; Progress, challenges and applications*, Wageningen UR Frontis Series: 6. 74, Kluwer Academic Publishers, Dordrecht, The Netherlands, pp. 95-141.
- Frusciante L., Barone A., Carputo D., Ercolano M.R., della Rocca F., Esposito S. 2000. Evaluation and use of plant biodiversity for food and pharmaceuticals. *Fitoterapia*, 71:S66-S72.
- Hassan S.B.M., Dragonetti G., Comegna A., Sengouga A., Lamaddalena N., Coppola A. 2022. A bimodal extension of the ARYA&PARIS approach for predicting hydraulic properties of structured soils. *J. Hydrol.* 610:127980.
- Jarvis P.G., McNaughton K.G. 1986. Stomatal control of transpiration: Scaling up from leaf to region. In: MacFadyen A., Ford E.D. (Eds.) *Advances in ecological research.* Vol. 15, Academic Press, London, UK, pp. 1-49.
- Jarvis P.G., Monteith J.L., Weatherley P.E. 1976. The interpretation of the variations in leaf water potential and stomatal conductance found in canopies in the field. *Philos. T. Roy. Soc. B.* 273:593-610.
- Knight J.H. White I. Zegelin S.J. 1995. Sampling volume of TDR probes used for water content monitoring. *Proc. Symp. Workshop on Time Domain Reflectometry.* Env. Infrastruct. Min. Appl. Evanston, IL, USA, SP 19-94: 93-104
- Li X., Yang P., Ren S., Li Y., Liu H., Du J., Li P., Wang C., Ren L. 2010. Modeling cherry orchard evapotranspiration based on an improved dual-source model. *Agr. Water Manag.* 98:12-8.
- Marino G., Pallozzi E., Coccozza C., Tognetti R., Giovannelli A.,

- Cantini C., Centritto M. 2014. Assessing gas exchange, sap flow and water relations using tree canopy spectral reflectance indices in irrigated and rainfed *Olea europaea* L. *Environ. Exp. Bot.* 99:43-52.
- Molz F.J. 1981. Models of water transport in the soil-plant system: A review. *Water Resour. Res.* 17:1245-60.
- Monteith J., Unsworth M. 2013. Principles of environmental physics: plants, animals, and the atmosphere. 4th ed. Academic Press, Oxford, UK.
- Mu Q., Zhao M., Running S.W. 2011. Improvements to a MODIS global terrestrial evapotranspiration algorithm. *Remote Sens. Environ.* 115:1781-800.
- Parkinson K.J. 1983. Porometry in S.E.B. Symp. instrumentation for environmental physiology, Cambridge, UK.
- PP Systems. 2017. CIRAS-3 Portable photosynthesis system operation manual. Version 1. PP Systems, Amesbury, Massachusetts, US.
- Roose T., Fowler A.C. 2004. A model for water uptake by plant roots. *J. Theor. Biol.* 228:155-71.
- Rudich J., Kalmar D., Geizenberg C. and Harel S. 1977. Low water tensions in defined growth stages of processing tomato plants and their effects on yield and quality. *J. Hortic. Sci.* 52:391-9.
- Russo D., 1988. Determining soil hydraulic properties by parameter estimation: On the selection of a model for the hydraulic properties. *Water Resour. Res.* 24:453-9.
- Schaap M.G., Robinson D.A., Friedman S.P., Lazar A. 2003. Measurement and modeling of the TDR signal propagation through layered dielectric media. *Soil Sci. Soc. Am. J.* 61: 1113-21.
- Schröder T., Javaux M., Vanderborght J., Körfgen B., Vereecken H. 2008. Effect of local soil hydraulic conductivity drop using a three-dimensional root water uptake model. *Vadose Zone J.* 7:1089-98.
- Severino G., Coppola A. 2013. A note on the apparent conductivity of stratified porous media in unsaturated steady flow above a water table. *Transp. Porous Med.* 91:733-40.
- Shuttleworth W.J. 2007. Putting the 'vap' into evaporation. *Hydrol. Earth Syst. Sc.* 11:210-44.
- Shuttleworth W.J., Wallace J.S. 1985. Evaporation from sparse crops-an energy combination theory. *Q. J. Roy. Meteor. Soc.* 111:839-55.
- Sillo F., Marino G., Franchi E., Haworth M., Zampieri E., Pietrini I., Fusini D., Mennone C., Centritto M., Balestrini R. 2022. Impact of irrigation water deficit on two tomato genotypes grown under open field conditions: From the root-associated microbiota to the stress responses. *Ital. J. Agron.* 17:2130.
- Šimůnek J., van Genuchten M.T. 1996. Estimating unsaturated soil hydraulic properties from tension disc infiltrometer data by numerical inversion. *Water Resour. Res.* 32:2683-96.
- Šimůnek J., van Genuchten M.T., Sejna M. 2008. Development and applications of the HYDRUS and STANMOD software packages and related codes. *Vadose Zone J.* 7:587-600.
- Topp, G.C., Ferré, P.A. 2002. The soil solution phase. In: Dane J.H., Topp G.C., Campbell G.S. (Eds.) *Methods of soil analysis. Part 4. Physical methods.* SSSA Book series No. 5, Madison, WI, USA, pp. 417-545.
- van Dam J.C., Huygen J., Wesseling J.G., Feddes R.A., Kabat P., van Walsum P.E. V, Groenendijk P., van Diepen C.A. 1997. Theory of SWAP version 2.0; Simulation of water flow, solute transport and plant growth in the soil-water-atmosphere-plant environment. Technical Doc. 45. Wageningen Agricultural University and DLO Winand Staring Centre. Wageningen, The Netherlands.
- van Genuchten M.T. 1980. A closed-form equation for predicting the hydraulic conductivity of unsaturated soils. *Soil Sci. Soc. Am. J.* 44:892-8.
- von Caemmerer S., Farquhar G.D. 1981. Some relationships between the biochemistry of photosynthesis and the gas exchange of leaves. *Planta.* 153:376-87.
- Warrick A.W. 1974. Time-dependent linearized infiltration. I. Point sources. *Soil Sci. Soc. Am. J.* 38:383-6.
- Williams M., Rastetter E.B., Fernandes D.N., Goulden M.L., Wofsy S.C., Shaver G.R., Melillo J.M., Munger J.W., Fa S.M., Nadelhoffer K.J. 1996. Modelling the soil-plant-atmosphere continuum in a *Quercus* – *Acer* stand at Harvard Forest: the regulation of stomatal conductance by light, nitrogen and soil/plant hydraulic properties. *Plant Cell Environ.* 19:911-27.